IEEE Photonics Journal
An IEEE Photonics Society Publication

Open Access

A 51.6 Mb/s Experimental VLC System Using a Monochromic Organic LED

Volume 10, Number 2, April 2018

Hanjie Chen
Zhengyuan Xu
Qian Gao
Shangbin Li

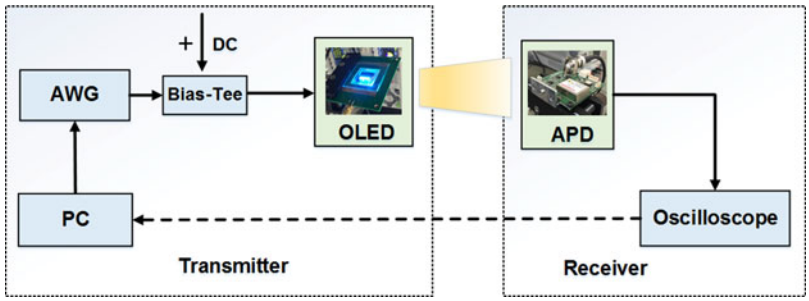

DOI: 10.1109/JPHOT.2017.2748152
1943-0655 © 2017 IEEE

IEEE photonics SOCIETY

IEEE

A 51.6 Mb/s Experimental VLC System Using a Monochromic Organic LED

Hanjie Chen,[1] Zhengyuan Xu,[1, 2] Qian Gao,[1] and Shangbin Li[1]

[1]Key Laboratory of Wireless-Optical Communications, Chinese Academy of Sciences, School of Information Science and Technology, University of Science and Technology of China, Hefei 230027, China
[2]Shenzhen Graduate School, Tsinghua University, Shenzhen 518055, China

DOI:10.1109/JPHOT.2017.2748152

Manuscript received July 14, 2017; revised August 26, 2017; accepted August 29, 2017. Date of publication September 1, 2017; date of current version February 28, 2018. This work was supported in part by National Key Basic Research Program of China under Grant 2013CB329201, in part by the Key Program of National Natural Science Foundation of China under Grant 61631018, in part by the Key Research Program of Frontier Sciences of CAS under Grant QYZDY-SSW-JSC003, in part by the Key Project in Science and Technology of Guangdong Province under Grant 2014B010119001, and in part by Shenzhen Peacock Plan under Grant 1108170036003286. Corresponding author: Zhengyuan Xu (e-mail: xuzy@ustc.edu.cn).

Abstract: An organic light emitting diode (OLED) shows characteristics different from a traditional semiconductor LED when both are applied to visible light communication (VLC). This paper first experimentally characterizes its static and dynamic communication properties with varying input signals. This band-limited and power-limited light source leads to unique communication channel and noise models. Accordingly, the orthogonal frequency-division multiplexing in conjunction with offset quadrature amplitude modulation (OFDM-OQAM) is applied, and its performance is compared against the traditional dc-biased optical OFDM. To further enhance the communication performance, a bit and power loading algorithm and a proper equalization algorithm are jointly implemented to combat the channel frequency selectivity and increase the data rate. A bit-rate of 51.6 Mb/s based on a monochromic OLED is experimentally achieved through the proposed design. The rate is comparable to the multicolor OLEDs-based VLC link in the literature.

Index Terms: Organic LED, VLC, dynamic transfer characteristic, OFDM-OQAM, bit and power loading.

1. Introduction

Organic light emitting diodes (OLEDs) have been widely used in lighting and display products, with several attractive features including flexibility, easy integration and fabrication, rich colors, and wide beaming angle. Recently, some studies have shown that OLEDs can serve as optical transmitters in visible light communications (VLC) [1]–[4]. But the lower cut-off frequency of OLEDs is a key disadvantage, which limits the transmission data rate compared with LED-based systems.

Properties of OLEDs can be improved through developing new materials with high charge mobility and applying meliorative manufacturing techniques [5], [6]. The response speed of organic devices is thus increased. In addition to bandwidth expansion, advanced communication techniques also help to increase data rate, including orthogonal frequency division multiplexing (OFDM), multiple-input-multiple-output (MIMO), and equalization [7]–[9]. The transmission rate has significantly increased

from Mbps to tens of Mbps over the past years [10]–[12]. Up to now, the highest data rate of an organic VLC system reaches as high as 55 Mbps [13]. It utilizes multicolor OLEDs and applies wavelength division multiplexing (WDM) with a multilayer perceptron artificial neural network (MLP-ANN) equalizer. The blue, red and green OLEDs deliver data rates of 27.9 Mbps, 18.6 Mbps and 8.4 Mbps respectively.

In fact, characterization of organic devices for VLC is an essential step towards system design and performance study [14]. According to our preliminary experiments, OLEDs have a much larger linear dynamic range than traditional LEDs [15]. Thus the driving signal is allowed to vary in a relatively large scale without incurring obvious nonlinear effects. This characteristic is advantageous and promising for VLC as compared to traditional LEDs, especially when a nonlinearity sensitive modulation such as OFDM is used. The OFDM combined with offset quadrature amplitude modulation (OFDM-OQAM) is a bandwidth-efficient modulation scheme. It is not only successfully used in radio frequency (RF) and optical fiber communication (OFC) [16]–[18], but also adopted for VLC to increase data rate [19].

According to [13], the blue OLED can deliver the highest data rate among three colors of OLEDs. Meanwhile, the blue OLED has the largest bandwidth based on our experimental test on available blue, red and green OLEDs. In this paper, we build an experimental VLC system utilizing a blue light OLED at the transmitter and an avalanche photodiode (APD) at the receiver. First, we focus on the primary OLED-based VLC system. The channel and noise models are established on the basis of measurement results to analyze the link performance. Based on the transfer characteristics of the link, the peak-to-peak voltage (V_{pp}) and bias voltage (V_{DC}) are suitably chosen to ensure linear operation of the device and better signal to noise ratio (SNR). Subsequently, we address transmitter and receiver design for better communication performance. We propose a modified OFDM-OQAM where the modulation and demodulation are conveniently performed through inverse fast Fourier transform (IFFT) and FFT. This efficient implementation is different from the filter-bank based OFDM-OQAM, while still inherits its appealing features. Time-frequency well-placed prototype filters help to suppress sidebands and compensate channel dispersion, and enhance robustness to interference than the traditional OFDM [20], [21]. The proposed OFDM-OQAM design also discards cyclic prefix (CP) to improve spectral efficiency over the traditional DC-biased optical OFDM (DCO-OFDM) [22]. Noticing the frequency selectivity of the OLED communication channel, we apply a bit/power loading algorithm jointly with OFDM-OQAM at the transmitter to match the device frequency characteristics and mitigate frequency selective distortions.

To ensure high data rate under the bit error rate (BER) requirement, a joint linear minimum mean-square-error (LMMSE) and decision feedback equalizer (DFE) is further applied at the receiver to combat possible inter-symbol interference (ISI) and intercarrier interference (ICI) due to limited bandwidth and nonlinearity of the OLED. By the proposed design and implementation, a data rate of 51.6 Mbps is achieved for the BER below the 7% forward error correction (FEC) limit of 3.8×10^{-3}, which is comparable to the 3-color OLED-based VLC link and much higher than the monochronic OLED-based VLC link reported in the literature.

The rest of the paper is organized as follows. In Section 2, the performance of the basic organic VLC system is studied, including electrical and optical properties of the OLED, link transfer characteristics and SNR. Section 3 presents the advanced design methods of optical OFDM/OQAM, bit/power loading, and channel equalization for a high-speed organic VLC system. The experimental performance of the designed system is demonstrated in Section 4. Finally, Section 5 concludes the paper.

2. Characteristics and Performance of the Basic Organic VLC System

The basic organic VLC system is designed and experimentally set up, as Fig. 1 shows. A blue light OLED and an APD act as the transmitter and the receiver respectively. The OLED in our experiments is a customized device produced by Visionox company. We examine the electrical and optical characteristics of the adopted device for subsequent system design.

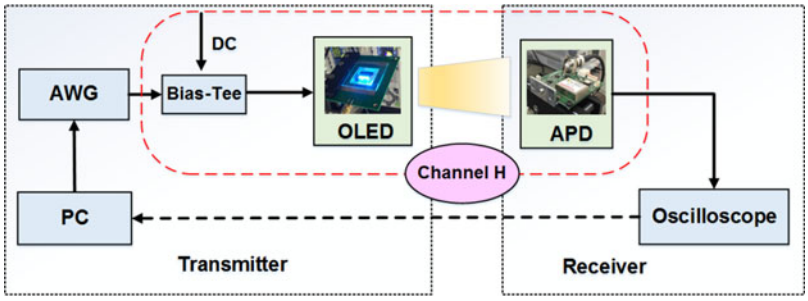

Fig. 1. Experimental system diagram.

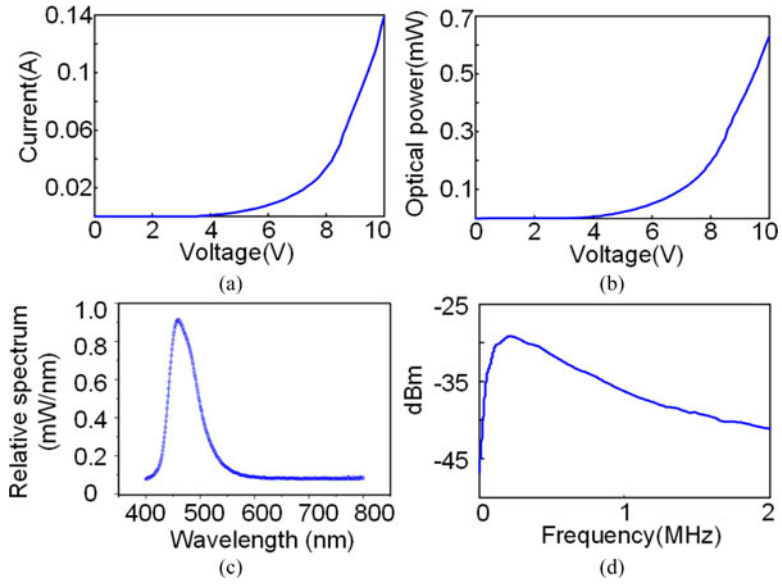

Fig. 2. OLED characteristics. (a) I-V curve. (b) P-V curve. (c) Normalized optical spectrum. (d) Frequency response.

2.1. OLED Characteristics

The luminous area of the OLED is as small as $0.3 \times 1.2\,\text{cm}^2$. Its measured I-V and P-V curves are depicted in Fig. 2(a) and 2(b) respectively, where I is the forward current, V is the bias voltage, and P is the output optical power measured by an optical power meter (THORLABS PM 130D). The bias voltage leading to the maximum quasi-linear operation range is found to be about 9 V, much larger than that of a traditional illuminative LED. But the optical power is far smaller, showing a power-limited property. Fig. 2(c) plots the normalized optical spectrum measured by a spectrum analysis system (EVERFINE Integrating Sphere) under a normal bias voltage. The peak wavelength is found about 462 nm.

We also examine the electrical bandwidth of the device. The bandwidth of the adopted APD (HAMAMATSU C10508) from DC to 10 MHz is much larger than the OLED and thus imposes negligible effect on the overall link bandwidth since an OLED typically shows bandwidth in the order of sub-MHz. An arbitrary waveform generator (AWG, ROGOL DG5252) produces a swept-frequency signal ranging from 1 Hz to 2 MHz with V_{pp} 100 mV. The signal is applied to the OLED via a bias-tee (PRL-BTAC-114L), in which the AC voltage is superimposed onto the DC operating voltage of the OLED. At the receiver, the APD output signal is captured by a spectrum analyzer (RIGOL DSA1030A). The signal spectrum is recorded and displayed, as Fig. 2(d) shows. The 3 dB bandwidth of the OLED under a normal operating condition is found to be 460 kHz, which indicates the narrowband characteristic, much smaller than a traditional LED.

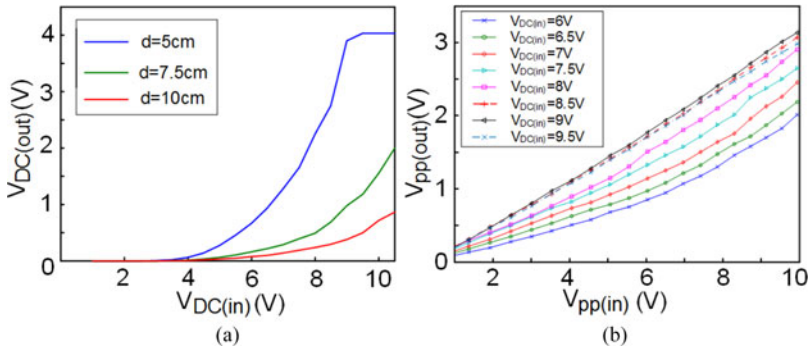

Fig. 3. (a) Static transfer characteristics. (b) Dynamic transfer characteristics.

2.2. System Transfer Characteristics

An OLED may operate in a static mode without input signal variation or dynamic mode with a time-varying input signal. The front-end transfer characteristics depend on the OLED operation modes. The static and dynamic transfer characteristics of the organic link refer to those corresponding to DC and AC driving signals respectively. According to the static transfer characteristic curves in Fig. 3(a), the APD nearly has no response until the OLED bias voltage ($V_{DC(in)}$) reaches the threshold. Then the APD output voltage ($V_{DC(out)}$) increases dramatically with the growth of the OLED bias voltage, which represents the static nonlinearity. When the transmitter and receiver separation distance is short ($d = 5$ cm), the APD tends to be saturated as the OLED bias voltage increases to its upper limit. As the distance increases, the APD would not be saturated even with a large LED bias voltage, at the cost of decrease of the received signal intensity.

The situation changes when the OLED sends an AC signal. Fig. 3(b) shows the output responses of the APD when the $V_{pp(in)}$ of a 100 kHz sine wave signal increases from 1 to 10 V, the largest value that the AWG can load to the OLED. According to the curves ($bias\,voltage = 6 \sim 9V$), the received $V_{pp(out)}$ increases with both increased input AC $V_{pp(in)}$ and increased bias voltage (when the bias voltage is not larger than 9.5 V). This result builds a link between dynamic and static operation conditions of the OLED. When the bias voltage is further increased to 9.5 V which is beyond the linear operation point of the OLED, the received $V_{pp(out)}$ begins to decrease as compared with $bias\,voltage = 9$ V. The curve ($bias\,voltage = 9$ V) is nearly linear, which shows a large linear dynamic range of the link.

2.3. Organic VLC System Performance

In view of the linear dynamic transfer characteristics of the organic link, the input/output relationship can be denoted as $y = h \otimes x$, where x and y are the input and output signals, and h is the channel impulse response. As for the multi-carrier signal, $X = [X_1, X_2, \cdots, X_N]^T$, where N is the number of subcarriers. The attenuation coefficients of different sub-channels can be stacked into a vector $H = [H_1, H_2, \cdots, H_N]^T$. The output signal becomes $Y = H^T X$.

The channel is estimated by transmitting a long Zadoff-Chu sequence. A block-type pilot structure is adopted, as Fig. 4(a) shows, to obtain the accurate information of each sub-channel. To meet the constraints that the optical intensity-modulated signal must be real and positive, the pilot sequences should satisfy the Hermitian symmetric property in the frequency domain. The channel is from the AWG output end to the oscilloscope (AGILENT 6004A) receiving end. Those factors in the link, including the low-frequency cutoff of the bias-tee, the impedance matching and electro-optical conversion of the OLED, the propagation channel between the OLED and the APD, the photoelectric conversion, and amplification in APD, all have contributions to the channel coefficient H. When SNR is high, each sub-channel coefficient, as Fig. 4(b) shows, can be estimated by averaging the estimates from a sufficiently long training sequence.

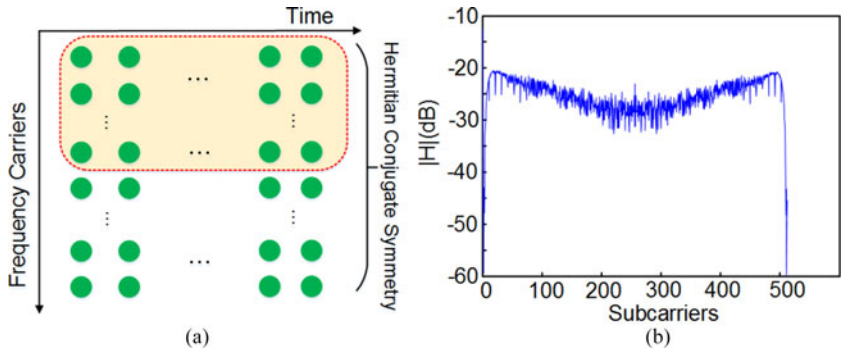

Fig. 4. (a) The pilot structure. (b) Channel coefficients.

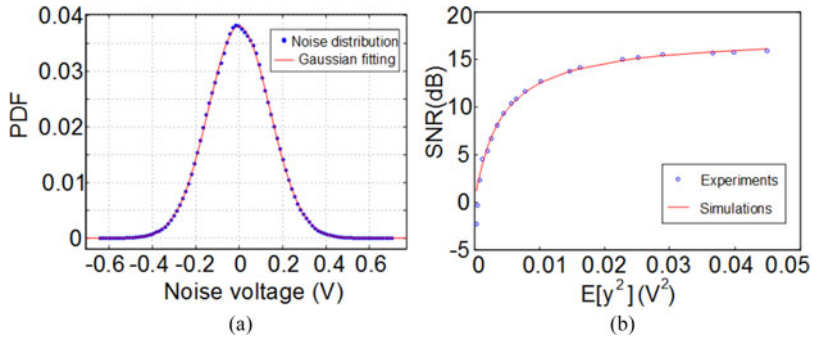

Fig. 5. (a) Noise distribution. (b) The relationship between the receiver SNR and the signal power.

The received signal $r(n)$ is the output signal $y(n)$ corrupted by noise $w(n)$, $r(n) = y(n) + w(n)$, where the time domain signal $y(n) = h(n) \otimes x(n)$. In the organic system, the noise $w(n)$ contains signal-dependent noise $v(n)$ and signal-independent noise $u(n)$. The signal-dependent noise mainly includes the shot noise brought by the APD, and the signal-independent noise includes thermal noise and background noise. We do not consider the truncation noise caused by nonlinearity given the good linear dynamic transfer characteristic of the system.

The multi-carrier signal, $x(n) = IFFT\{X(k)\}$, follows the Gaussian distribution according to the central limit theorem. The output signal $y(n)$ is a linear superposition of the signals from different subcarriers, and thus also follows the Gaussian distribution. As $y \sim \mathcal{N}(\mu, \sigma^2)$, the signal power at the receiver is $E[y^2] = \mu^2 + \sigma^2$. The noise power is

$$\begin{aligned} E[w^2] &= E[v^2] + E[u^2] = k^2 E[y^2] + \sigma_u^2 \\ &= k^2(\mu^2 + \sigma^2) + \sigma_u^2, \end{aligned} \tag{1}$$

where k is a scalar describing the dependence of the noise on the signal. The SNR at the receiver can be expressed as

$$\text{SNR} = 10 \log \left(\frac{E[y^2]}{E[w^2]} \right) = 10 \log \left(\frac{1}{k^2 + \frac{\sigma_u^2}{E[y^2]}} \right). \tag{2}$$

The noise can be separated from the received signal once contribution from the training signal is reconstructed from estimated channel parameters.

The measured noise probability distribution function (PDF) is depicted in Fig. 5(a), which shows a good fitting with the Gaussian distribution. The SNR at the receiver can be estimated by sending a BPSK modulated training sequence [23]. With the increase of the transmitted signal V_{pp} from 1 V to 10 V, the experimental SNRs changing with the received signal power are shown in Fig. 5(b).

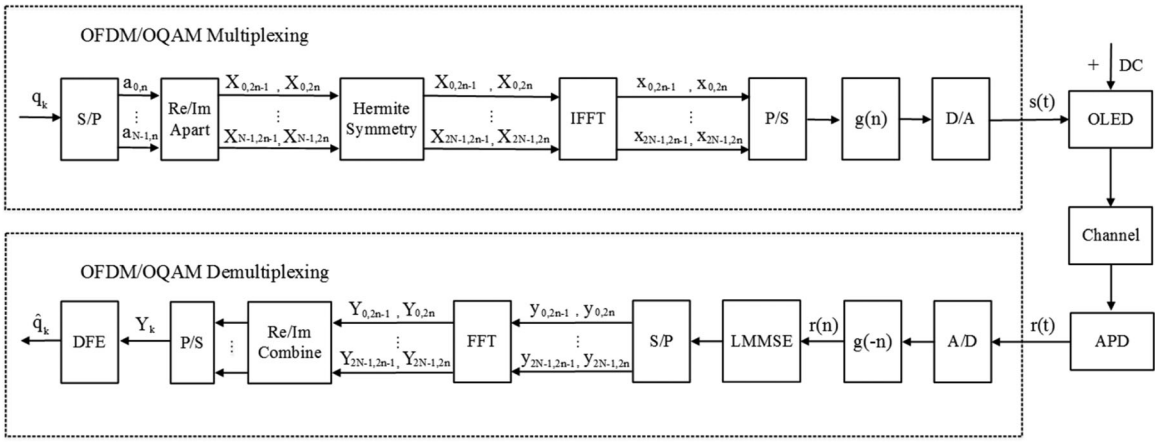

Fig. 6. Block diagram of the optical OFDM-OQAM.

The relationship is consistent with the simulation results based on (2), which validates the above models. The SNR first increases then tends to be saturated with the increase of the signal power. There is no apparent decline of the SNR caused by the truncation noise brought by nonlinearity, which is quite different from the traditional LED systems [24], [25]. It demonstrates that OLED has a larger linear dynamic range than LED, which entails more capabilities to modulation design for an OLED-based VLC system. Explorations in the above characteristics of the organic communication link help to adjust the system to an appropriate operation condition, including the optimal bias voltage and peak-to-peak voltage.

3. Design of a High-Speed Organic VLC System

The previous OLED-based VLC system consists of basic building blocks. Its performance is limited by the OLED bandwidth. Thus advanced modulation and bit/power loading methods are proposed at the transmitter to match the device frequency characteristics and transmit signals efficiently through the channel. At the receiver, the limited channel bandwidth and residual non-linearity cause possible ISI and ICI. A joint LMMSE and DFE is applied to tackle those issues.

3.1. FFT/IFFT Based Optical OFDM-OQAM

To maximize the spectral efficiency of the bandwidth-limited system and adequately utilize the linear dynamic transfer characteristic, multi-carrier modulation is considered. Compared with the traditional DCO-OFDM, the OFDM-OQAM shows better performance in suppressing the high out-of-band spectrum leakage and the data rate is further increased by removing cyclic prefix.

The block diagram of the proposed FFT/IFFT based optical OFDM-OQAM is illustrated in Fig. 6. The transmitted signal can be expressed as

$$s(t) = \sum_{n=-\infty}^{n=+\infty} \sum_{m=0}^{N-1} a_{m,n} g_{m,n}(t), \tag{3}$$

where $a_{m,n}$ is the transmitted data on the mth subcarrier of the nth symbol. And $g_{m,n}(t)$ is the prototype filter function at time-frequency lattice (m, n), $g_{m,n}(t) = e^{j2\pi m\nu_0 t} g(t - n\tau_0)$, where ν_0 is the gap between subcarriers, τ_0 is the time migration between the real and imaginary parts of a symbol. This parameter is related to the symbol period T and the subcarrier spacing F of a traditional OFDM symbol as $T = 2\tau_0 = \frac{1}{F} = \frac{1}{\nu_0}$.

In order to restore the original sending data a_{m_0,n_0} at the receiver by the following,

$$\begin{aligned}\hat{a}_{m_0,n_0} &= \langle s(t), g_{m_0,n_0}\rangle_{\Re} \\ &= \sum_{n=-\infty}^{n=+\infty}\sum_{m=0}^{N-1} a_{m,n}\langle g_{m,n}, g_{m_0,n_0}\rangle_{\Re} \\ &= \sum_{n=-\infty}^{n=+\infty}\sum_{m=0}^{N-1} a_{m,n}\delta_{m,m_0}\delta_{n,n_0} = a_{m_0,n_0},\end{aligned} \tag{4}$$

the prototype filter function should meet the orthogonal condition in the real domain, $\langle g_{m,n}, g_{m_0,n_0}\rangle_{\Re} = \delta_{m,m_0}\delta_{n,n_0}$, which relaxes the strict orthogonality of the OFDM. In our experiments, $g(t)$ is designed to be a square-root raised cosine filter with a roll-off factor of 0.5.

To reduce the complexity and cost, the OFDM-OQAM system is realized by an efficient FFT/IFFT-based implementation. The plural symbols $[a_{0,n}, a_{1,n}, \cdots, a_{N-1,n}]^T$ mapped from bit streams are split into the real part $[X_{0,2n-1}, X_{1,2n-1}, \cdots, X_{N-1,2n-1}]^T$ and the imaginary part $[X_{0,2n}, X_{1,2n}, \cdots, X_{N-1,2n}]^T$. The two parts are transmitted respectively within a time period. To obtain a real-valued signal, $X(n)$ should satisfy the Hermitian symmetry before the IFFT, that is $X_{m,n} = X^*_{2N-m,n}$, $0 < m < N$. Then the signal $x(n)$ in the time domain can be obtained after the IFFT. After parallel to serial conversion, pulse shaping filtering and digital to analog conversion, the transmitted signal $s(t)$ is produced.

For a discrete system, $t = t_0 + i\tau_0$, $s(t) = s(t_0 + i\tau_0) = s[i]$, the transmitted real and positive signal $s[i]$ can be expressed as (5). Then a DC bias is added to drive the OLED.

$$\begin{aligned}s[i] &= \Re\left\{\sum_{n=-\infty}^{n=+\infty}\sum_{m=0}^{N-1}\left[a_m(n)^{\Re} g_m(i-(2n-1)) + a_m(n)^{\Im} g_m(i-2n)\right]\right\} \\ &= \Re\left\{\sum_{n=-\infty}^{n=+\infty}\sum_{m=0}^{N-1}\left[e^{j2\pi m\nu_0(2n-1)} X_m(2n-1)g(i-(2n-1)) + e^{j2\pi m\nu_0(2n)} X_m(2n)g(i-2n)\right]\right\} \\ &= \frac{1}{2}\sum_{n=-\infty}^{n=+\infty}\left\{\left[\sum_{m=0}^{N-1}(e^{j2\pi m\nu_0(2n-1)} X_m(2n-1) + e^{-j2\pi m\nu_0(2n-1)} X^*_m(2n-1))\right] g(i-(2n-1))\right. \\ &\quad \left. + \left[\sum_{m=0}^{N-1}\left(e^{j2\pi m\nu_0(2n)} X_m(2n) + e^{-j2\pi m\nu_0(2n)} X^*_m(2n)\right)\right] g(i-2n)\right\} \\ &= \frac{1}{2}\sum_{n=-\infty}^{n=+\infty}\left\{\left[\sum_{m=0}^{2N-1} e^{j2\pi m\nu_0(2n-1)} X_m(2n-1)\right] g(i-(2n-1)) + \left[\sum_{m=0}^{2N-1} e^{j2\pi m\nu_0(2n)} X_m(2n)\right] g(i-2n)\right\} \\ &= \frac{1}{2}\sum_{n=-\infty}^{n=+\infty}\left\{x(2n-1)g(i-(2n-1)) + x(2n)g(i-2n)\right\} \\ &= \sum_{n=-\infty}^{n=+\infty}[x(n)g(i-n)] = x(i)\otimes g(i).\end{aligned} \tag{5}$$

3.2. Bit and Power Loading

In our experiments, the channel is frequency selective, and the system performance is significantly degraded by those subcarriers with low SNRs. Therefore, a practical bit and power loading algorithm [26] is applied to improve the BER performance. During the process, an optimal system performance margin γ is determined first. Then the algorithm performs a recursive calculation and adjusts power distribution according to the channel coefficients. For our experimental VLC system, the channel

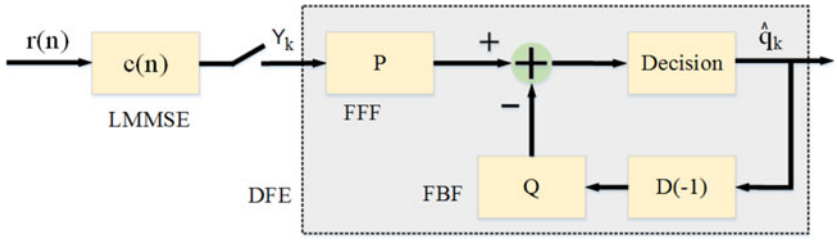

Fig. 7. Equalizer structure.

exhibits a low-pass property, which means the subcarriers in the high-frequency range would experience deep decay in signal power. So we estimate SNR of the experimental channel to find an appropriate γ. A method in [23] is very efficient by calculating the error vector magnitude (EVM) as follows

$$\text{SNR} \approx \frac{1}{(EVM)^2}. \tag{6}$$

For a normalized constellation, EVM is defined as root-mean-square (RMS) value of the difference between all ideal symbols and demodulated symbols [27]. Usually, those differences are averaged over a given large number of symbols. The square of EVM is often shown as a percentage of average power per symbol of the constellation and is expressed as

$$\text{EVM} = \left[\frac{\frac{1}{M}\sum_{k=1}^{M} |S_{ideal,k} - Y_{real,k}|^2}{\frac{1}{M}\sum_{k=1}^{M} |S_{ideal,k}|^2} \right]^{\frac{1}{2}}, \tag{7}$$

where $S_{ideal,k}$ is the ideal normalized constellation point for the kth symbol, $Y_{real,k}$ is the kth normalized measured symbol, and M is the number of total symbols.

Given the measured channel SNR and target BER, the bit and power loading algorithm would dynamically allocate bits and power on each subcarrier according to the following

$$b(i) = \log_2\left(1 + \frac{SNR(i)}{\xi + \gamma}\right), \tag{8}$$

where $b(i)$ is the number of bits allocated to the ith subcarrier, $SNR(i)$ is the measured SNR of the ith subcarrier, ξ is the "SNR gap" in the well-known "gap approximation" related to the target BER [28], and γ is an adjusting parameter. It is iteratively updated at a certain small step size under a total power constraint

$$\max\left(\sum_{i=1}^{N} b(i)\right) \text{ subject to } \sum_{i=1}^{N} P_i \leq P_{\max}, \tag{9}$$

where N denotes the number of subcarriers carrying information, and P_i represents the ith subcarrier power. The total signal power is limited by $P_{\max}$. After the above operations, fewer or none bits would be allocated to the low-SNR subcarriers, while more bits to high-SNR subcarriers.

At the receiver, after analog to digital conversion and filtering, the signal $r(n)$ first passes through a linear LMMSE equalizer. Then after serial-to-parallel conversion and FFT, the real part $[Y_{0,2n-1}, Y_{1,2n-1}, \cdots, Y_{2N-1,2n-1}]^T$ and the image part $[Y_{0,2n}, Y_{1,2n}, \cdots, Y_{2N-1,2n}]^T$ are recombined and the conjugate redundant parts are removed. Finally, a decision feedback equalizer (DFE) is employed to restore the original information symbols.

3.3. Equalization

The equalizer used in this work is a discrete-time LMMSE equalizer adding with a DFE equalizer. The structure is shown in Fig. 7. Compared with zero-forcing equalizer, LMMSE equalizer performs

better in minimizing the noise induced error [29]. Considering the frequency selective channel, DFE equalizer can eliminate ISI and ICI efficiently [30], [31].

This kind of LMMSE equalizer belongs to the class of Wiener filters. The principle is to minimize the mean square error between the desired signal and equalized signal

$$\arg\min E[\|s(n) - c(n) \otimes r(n)\|^2], \tag{10}$$

where $s(n)$ is the desired signal, $r(n)$ is the received signal, and $c(n)$ is a set of filter coefficients. The filter coefficients depending on channel impulse response can be determined by training symbols

$$c(n) = R_{rr}^{-1} R_{rs}, \tag{11}$$

where R_{rr} is the autocorrelation of the received signal, and R_{rs} is the cross-correlation between the received signal and the training signal.

The time-domain LMMSE equalizer can preliminarily equalize the non-flat channel. To further increase data rate, a symbol-level DFE equalizer is designed using a feedforward filter (FFF), a feedback filter (FBF), and a symbol delay module (D(−1)) with an adaptive algorithm. The original signal $\boldsymbol{q}_k = [q_{k,1}, q_{k,2}, \cdots, q_{k,N}]^T$, where $q_{k,i}$ is the kth symbol of ith subcarrier. The output symbol can be expressed as

$$\hat{\boldsymbol{q}}_k = \boldsymbol{P}\,\boldsymbol{Y}_k - \boldsymbol{Q}\,\boldsymbol{q}_{k-1}, \tag{12}$$

where $\boldsymbol{P}$ is FFF and $\boldsymbol{Q}$ is FBF. The estimation error is $\boldsymbol{e}_k = \boldsymbol{q}_k - \hat{\boldsymbol{q}}_k$. Then $\boldsymbol{P}$ and $\boldsymbol{Q}$ are determined by minimizing the mean square error

$$\arg\min E\{\|\boldsymbol{e}(k)\|^2\}. \tag{13}$$

As we can see, the FFF and FBF are related to ISI and ICI, and a recursive least square (RLS) algorithm is used to update the filter taps.

4. System Performance

In our experiments, the OFDM-OQAM signal is generated in MATLAB. The number of the IFFT/FFT points is 512. A designed frame contains 23 OFDM-OQAM symbols, one synchronization symbol, and two training symbols. Restricted by the total sample points of the oscilloscope, 20 frames are collected in every experiment to obtain enough symbols. Then the OFDM-OQAM signal is sent to the AWG, which converts the digital signal to analog signal. And the output signal added with a DC bias is loaded to the OLED. At the receiver, the oscilloscope is used to observe and record the received signal of the APD output. After down-sampling, synchronization, channel estimation, and equalization, the bit streams are demodulated in MATLAB, and the BER is calculated by comparing the restored bit streams with the transmitted bits. The LMMSE equalizer has 30 taps, and the DFE equalizer has 24 feedforward taps and 16 feedback taps.

Considering the characteristics of OLED and communication link, the bias and peak-to-peak voltages are chosen as 9 V and 10 V respectively. The transmission distance is first set to 12.5 cm because of relatively low luminance of the adopted OLED, and the performance versus distance is studied later. The data rate is controlled by adjusting the exporting symbol period of the AWG, $\omega = D \times \frac{B}{L}$, where ω is the exporting bit rate of the transmitter, D is the sampling rate of the AWG, L is the length of the data frame, and B is the number of bits contained in the signal frame. Further performance enhancement can be achieved with a bit and power loading algorithm and effective equalizer in the experiment.

According to the frequency selectivity of the organic link as Fig. 8(a) shows, we divide the frequency band into small intervals and utilize those subcarriers at the highest index possible to ensure SNR for signal demodulation. Fig. 8(b) shows the allocated bits for different subcarriers. Fewer or none bits are allocated to the low-SNR subcarriers, while more bits to high-SNR subcarriers. The bit and power allocation algorithm helps to significantly decrease the overall BER to a level of 10^{-6}, as seen from Fig. 8(c).

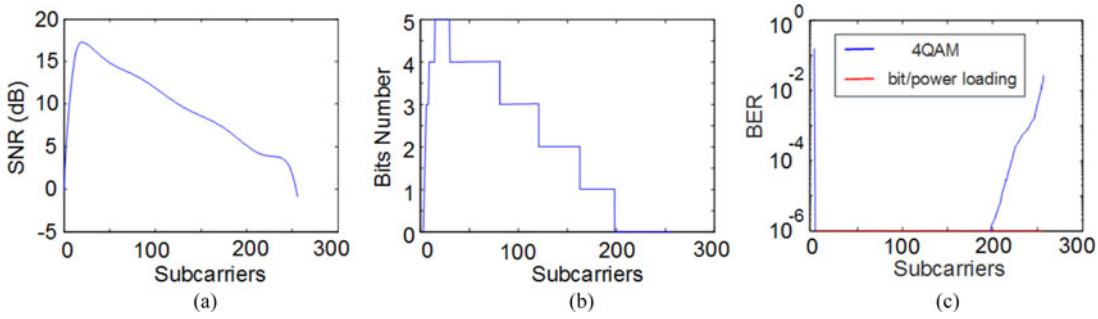

Fig. 8. OFDM/OQAM subcarrier performance and bit/power loading. (a) SNR on each subcarrier. (b) Bit allocation on subcarriers. (c) BER on each subcarrier.

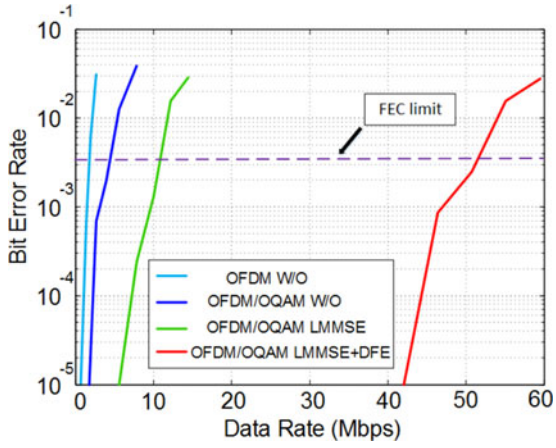

Fig. 9. BER versus data rate.

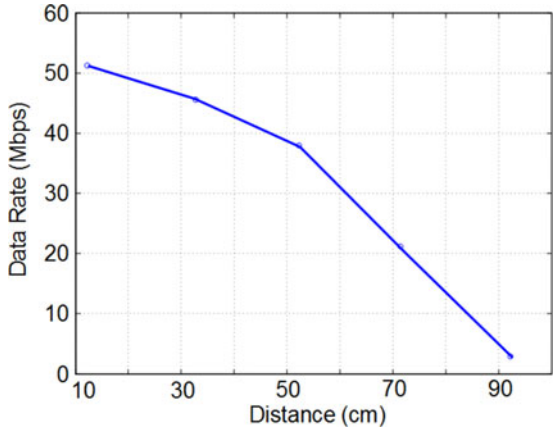

Fig. 10. Data rate versus communication distance.

The BERs corresponding to different data rates are tested, and results are shown in Fig. 9. As a comparison, the performance based on DCO-OFDM is presented as well. The modulation and demodulation of the DCO-OFDM signal are processed in MATLAB as OFDM-OQAM, and more details are available in [15]. When the target BER is set at 7% FEC limit 3.8×10^{-3}, a data rate of 4.8 Mbps is achieved for the OFDM-OQAM without equalizer added while only 2 Mbps for the DCO-OFDM. The performance can be improved dramatically with the joint LMMSE and DFE equalizers, and the maximum data rate can reach 51.6 Mbps. Thus, the ratio of data-rate over bandwidth is

about 112 times, which exceeds the highest 77 times of an on-off keying (OOK) based green light organic VLC link in [13] up to now. Therefore, our prototype shows better spectral efficiency of the bandwidth-limited system. Further data rate increase can follow wavelength-division multiplexing based on red/green/blue OLEDs as proposed in [13].

The experimental system is further tested when the communication distance between the transmitter and the receiver is increased. The achievable data rate versus distance is shown in Fig. 10. The performance deteriorates sharply with distance because the luminance of the OLED is relatively low. With assistance of a lens to increase SNR, the data rate goes over 10 Mbps when the distance is within 84 cm, considerable longer than 5 cm in most works of the existing literature. Another way to largely increase SNR is to utilize an arrayed OLED lighting panel, which will be studied in the future.

5. Conclusion

In this paper, we report the measured characteristics of the OLED from the communication perspective. Compared with the nonlinearity of LEDs, the linear dynamic transfer characteristics of the OLED show great potential for VLC applications. In view of the bandwidth limitation and the large linear dynamic range of the link, the OFDM-OQAM technique is applied jointly with a bit and power loading algorithm at the transmitter, and a proper equalizer at the receiver to recover transmitted signals. The proposed experimental system has achieved a high data rate of 51.6 Mbps.

References

[1] H. L. Minh, Z. Ghassemlooy, A. Burton, and P. A. Haigh, "Equalization for organic light emitting diodes in visible light communications," in *Proc. IEEE GLOBECOM Workshop*, Dec. 2011, pp. 828–832.

[2] H. Chun, C. J. Chiang, A. Monkman, and D. O. Brien, "A study of illumination and communication using organic light emitting diodes," *IEEE J. Lightw. Technol.*, vol. 31, no. 22, pp. 3511–3517, Nov. 2013.

[3] P. A. Haigh, Z. Ghassemlooy, S. Rajbhandari, and I. Papakonstantinou, "Visible light communications using organic light emitting diodes," *IEEE Commun. Mag.*, vol. 51, no. 8, pp. 148–154, Aug. 2013.

[4] W. H. Li *et al.*, "Squarylium and rubrene based filterless narrowband photodetectors for an all-organic two-channel visible light communication system," *Org. Electron.*, vol. 37, pp. 346–351, Oct. 2016.

[5] Y. Yao, Y. Y. Liang, V. Shrotriya, S. Q. Xiao, L. P. Yu, and Y. Yang, "Plastic near-infrared photodetectors utilizing low band gap polymer," *Adv. Mater.*, vol. 19, no. 22, pp. 3979–3983, Nov. 2007.

[6] W. Zhu *et al.*, "Graphene radio frequency devices on flexible substrate," *Appl. Phys. Lett.*, vol. 102, no. 23, Jun. 2013, Art. no. 233102.

[7] S. T. Le *et al.*, "10 Mb/s visible light transmission system using a polymer light-emitting diode with orthogonal frequency division multiplexing," *Opt. Lett.*, vol. 39, no. 13, pp. 3876–3879, Jul. 2014.

[8] P. A. Haigh *et al.*, "A mimo-ann system for increasing data rates in organic visible light communications systems," in *Proc. IEEE Int. Conf. Commun.*, Jun. 2013, pp. 5322–5327.

[9] P. A. Haigh, Z. Ghassemlooy, and H. L. Minh, "Exploiting equalization techniques for improving data rates in organic optoelectronic devices for visible light communications," *IEEE J. Lightw. Technol.*, vol. 30, no. 19, pp. 3081–3088, Oct. 2012.

[10] P. A. Haigh, Z. Ghassemlooy, and I. Papakonstantinou, "1.4-mb/s white organic led transmission system using discrete multitone modulation," *IEEE Photon. Technol. Lett.*, vol. 25, no. 6, pp. 615–618, Feb. 2013.

[11] P. A. Haigh *et al.*, "A 10 Mb/s visible light communication system using a low bandwidth polymer light-emitting diode," in *Proc. 9th Int. Symp. Commun. Syst., Netw. Digit. Signal Process.*, Jul. 2014, pp. 999–1004.

[12] P. A. Haigh *et al.*, "A 20-Mb/s VLC link with a polymer LED and a multilayer perceptron equalizer," *IEEE Photon. Technol. Lett.*, vol. 26, no. 19, pp. 1975–1978, Jul. 2014.

[13] P. A. Haigh *et al.*, "Wavelength-multiplexed polymer leds: Towards 55 mb/s organic visible light communications," *IEEE J. Sel. Areas Commun.*, vol. 33, no. 9, pp. 1819–1828, Sep. 2015.

[14] P. Chvojka, P. Dvorak, P. Pesek, S. Zvanovec, P. A. Haigh, and Z. Ghassemlooy, "Characterization of the organic LED based visible light communications," in *Proc. 10th Int. Symp. Commun. Syst., Netw. Digit. Signal Process.*, Prague, Czech Republic, Jul. 2016, pp. 1–4.

[15] H. Chen *et al.*, "A 1.9 Mbps OFDM-based all-organic visible light communication system," in *Proc. IEEE Int. Conf. Commun. Syst.*, Dec. 2016, pp. 1–6.

[16] C. Li *et al.*, "Experimental demonstration of 429.96-Gb/s OFDM/OQAM–64QAM over 400-km SSMF transmission within a 50-GHz grid," *IEEE Photon. J.*, vol. 6, no. 4, pp. 1–8, Aug. 2014.

[17] Z. Li *et al.*, "Experimental demonstration of 110-gb/s unsynchronized band-multiplexed superchannel coherent optical ofdm/oqam system," *Opt. Exp.*, vol. 21, no. 19, pp. 21 924–21 931, Sep. 2013.

[18] X. Gao, W. Wang, X. G. Xia, E. K. S. Au, and X. You, "Cyclic prefixed OQAM-OFDM and its application to single-carrier FDMA," *IEEE Trans. Commun.*, vol. 59, no. 5, pp. 1467–1480, May 2011.

[19] B. Lin *et al.*, "Experimental demonstration of OFDM/OQAM transmission for visible light communications," *IEEE Photon. J.*, vol. 8, no. 5, Oct. 2016, Art. no. 7906710.
[20] H. Bölcskei, "Orthogonal frequency division multiplexing based on offset qam," in *Advances in Gabor Analysis*, Boston, MA, USA: Birkhäuser, 2003, pp. 321–352.
[21] L. Vangelista and N. Laurenti, "Efficient implementations and alternative architectures for OFDM-OQAM systems," *IEEE Trans. Commun.*, vol. 49, no. 4, pp. 664–675, Apr. 2001.
[22] J. Armstrong, "Ofdm for optical communications," *IEEE J. Lightw. Technol.*, vol. 27, no. 3, pp. 189–204, Feb. 2009.
[23] R. A. Shafik, M. S. Rahman, and A. R. Islam, "On the extended relationships among evm, ber and snr as performance metrics," in *Proc. Int. Conf. Elect. Comput. Eng.*., Dec. 2006, pp. 408–411.
[24] S. Dimitrov and H. Haas, "Information rate of OFDM-based optical wireless communication systems with nonlinear distortion," *IEEE J. Lightw. Technol.*, vol. 31, no. 6, pp. 918–929, Mar. 2013.
[25] H. E. R. Mesleh and H. Haas, "Led nonlinearity mitigation techniques in optical wireless OFDM communication systems," *J. Opt. Commun. Netw.*, vol. 4, no. 11, pp. 865–875, Nov. 2012.
[26] P. S. Chow, J. M. Cioffi, and J. A. C. Bingham, "A practical discrete multitone transceiver loading algorithm for data transmission over spectrally shaped channels," *IEEE Trans. Commun.*, vol. 43, no. 2–4, pp. 773–775, Feb.–Apr. 1995.
[27] M. D. McKinley, K. A. Remley, and M. Myslinski, "EVM calculation for broadband modulated signals," in *Proc. 64th ARFTG Conf. Dig.*, Dec. 2004, pp. 45–52.
[28] G. D. Forney and M. V. Eyuboglu, "Combined equalization and coding using precoding," *IEEE Commun. Mag.*, vol. 29, no. 12, pp. 25–34, Dec. 1991.
[29] S. Haykin, *Adaptive Filter Theory*. 4th ed. Englewood Cliffs, NJ, USA: Prentice-Hall, 2002.
[30] T. Komine, J. H. Lee, S. Haruyama, and M. Nakagawa, "Adaptive equalization system for visible light wireless communication utilizing multiple white led lighting equipment," *IEEE Trans. Wireless Commun.*, vol. 8, no. 6, pp. 2892–2900, Jun. 2009.
[31] J. M. Cioffi, G. P. Dudevoir, M. V. Eyuboglu, and G. D. Forney, "MMSE decision-feedback equalizers and coding. i. equalization results," *IEEE Trans. Commun.*, vol. 43, no. 10, pp. 2582–2594, Oct. 1995.